Preprints.org

Article

Not peer-reviewed version

A Comparative Study on the Methods of Predictor Extraction from Global Sea Surface Temperature Fields for Statistical Climate Forecast System

Yawei Cai and Xiangjun Shi *

Posted Date: 16 January 2025

doi: 10.20944/preprints202501.1259.v1

Keywords: SST predictors; extracting method; statistical climate forecast system

Preprints.org is a free multidisciplinary platform providing preprint service that is dedicated to making early versions of research outputs permanently available and citable. Preprints posted at Preprints.org appear in Web of Science, Crossref, Google Scholar, Scilit, Europe PMC.

Copyright: This open access article is published under a Creative Commons CC BY 4.0 license, which permit the free download, distribution, and reuse, provided that the author and preprint are cited in any reuse.

Preprints.org (www.preprints.org) | NOT PEER-REVIEWED | Posted: 16 January 2025 doi:10.20944/preprints202501.1259.v1

Disclaimer/Publisher's Note: The statements, opinions, and data contained in all publications are solely those of the individual author(s) and contributor(s) and not of MDPI and/or the editor(s). MDPI and/or the editor(s) disclaim responsibility for any injury to people or property resulting from any ideas, methods, instructions, or products referred to in the content.

Article

A Comparative Study on the Methods of Predictor Extraction from Global Sea Surface Temperature Fields for Statistical Climate Forecast System

Yawei Cai and Xiangjun Shi *

School of Atmospheric Sciences, Nanjing University of Information Science and Technology, Nanjing 210044, China

* Correspondence: shixj@nuist.edu.com

Abstract: Statistical climate forecast system typically does not use preceding global gridded sea surface temperature (SST) data directly; instead, they extract a single predictor (e.g., the Niño3.4 index) or multiple predictors (e.g., time series of several SST spatial modes). In this study, four different SST predictor extracting methods (one single-predictor method and three multiple-predictor methods) are comparatively analyzed within the same climate forecast platform incorporating either the linear regression (LR) model or the neural network (NN) forecast model. Rolling forecast experiments with the LR model show that, compared to a single strong SST predictor, only multiple predictors with more high-quality information (high signal-to-noise ratio) could improve the forecast skill. Sensitivity experiments also show that the influence of multiple-predictor extracting methods on forecast skill from the NN model is much weaker than that from the LR model. Moreover, whether or not multiple SST predictors are orthogonal might also affect the forecast skill. The above experiences provide a reference for establishing statistical climate forecast system based on preceding SST data.

Keywords: SST predictors; extracting method; statistical climate forecast system

1. Introduction

As a crucial component of the climate system, the ocean profoundly influences global climate through the exchange of heat, momentum, and matter with the atmosphere [1–3]. Meanwhile, the latest ocean state serves as a crucial foundation for short-term climate forecasts due to its large heat capacity and slower changes compared to atmospheric processes [4–6]. Particularly for a climate forecast with a lead time of more than three months, indicative signals mostly come from the ocean state [7–9]. Therefore, the sea surface temperature (SST), as a key variable representing ocean conditions, has been an essential input physical variable for statistical climate forecast systems [10–12].

Previous theoretical studies usually focus on the influence mechanism of a single SST variable (e.g., the Niño3.4 index) on climate forecasts [13–15]. A single SST variable (i.e., single predictor) is insufficient for a statistical climate forecast system to capture valuable indicative signals provided by global SST data [16,17]. Moreover, a statistical climate forecast system typically does not directly use all globally gridded SST variables [18,19]. One primary reason is the high correlation among the SST variables at adjacent grid points, which implies the presence of redundant information within the global gridded SST data. Additionally, if all the SST grid variables were employed as input predictors, the number of predictors (exceeding 1,000) would be excessively high relative to the limited sample size of climate observations (less than 100), possibly giving rise to a severe overfitting issue. Consequently, it is of great significance for a statistical climate forecast system to extract a certain number of suitable predictors from the global SST data.

© 2025 by the author(s). Distributed under a Creative Commons CC BY license.

Preprints.org (www.preprints.org) | NOT PEER-REVIEWED | Posted: 16 January 2025 doi:10.20944/preprints202501.1259.v1

Although previous studies introduced many statistical forecast models with a few SST predictors [20–25], few focused on methods for extracting SST predictors. This study will compare four different extracting methods (one single-predictor method and three multiple-predictor methods) based on the same climate forecast system, which encompasses both linear and nonlinear regressions. Through comparative experiments, we endeavor to explore the following issues. Firstly, does the multiple-predictor lead to a notably enhanced forecast skill as compared to the single-predictor? Secondly, do different extracting methods exert a pronounced influence on forecast skill? Finally, are the aforementioned analyses dependent on the specific forecast model employed?

Here, we developed a forecast system for the June Western Pacific Subtropical High Ridge Line (WPSHRL) based on the preceding winter SST, using both the traditional linear regression (LR) model and the commonly used neural network (NN) model. Using this climate forecast system, the influence of the SST predictor extracting method was investigated. This paper is organized as follows: Section 2 presents the SST data and predictor extracting methods. Section 3 introduces the forecast system and related techniques. Section 4 illustrates the comparison among these different extracting methods. Finally, Section 5 presents the discussion and Section 6 provides the conclusions of the paper.

2. Data and Preprocessing

2.1. Data and Preliminary Analyses

The monthly SST data from 1961 to 2022 were downloaded from the Physical Sciences Laboratory [26]. In this study, only the winter SST anomaly, encompassing December of the previous year, January, and February, was used to extract predictors. The June WPSHRL data, representing the mean latitude position of the isoline where 500 hPa zonal wind u=0 and ∂u/∂y>0 surrounded by the 588 dagpm contour [27], were obtained from the National Climate Center of China. Due to the unavailability of data after 2016, the June WPSHRL data for recent years were manually calculated based on ERA5 reanalysis data, following the same definition.

The winter SST displays notable decadal trends associated with global warming, whereas the June WPSHRL does not exhibit such trends (Figure 1). Before incorporating these variables into the forecast system, both the winter SST anomalies and the June WPSHRL were detrended using a 21-point moving average. Additionally, the detrended June WPSHRL data were normalized to the range of −1 to 1 (i.e., June WPSHRL index, hereafter referred to as WPSHRL). Based on the ranking of the WPSHRL from 1961 to 2022, the lowest and highest ~1/4 of years were identified as anomaly events. Among these 31 anomaly events, 16 were classified as low-WPSHRL years and 15 as high-WPSHRL years.

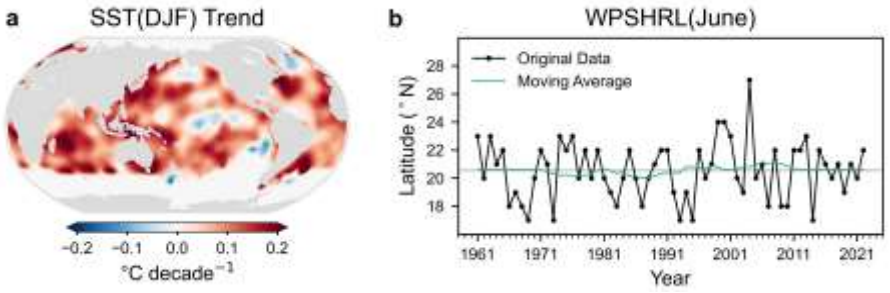

Figure 1. Decadal trends in SST and WPSHRL. (**a**) Spatial distribution of SST linear trends from 1961 to 2022. (**b**) Time series of original WPSHRL data (black) and 21-point moving averages (green).

To better understand the design concept underlying SST predictor extracting methods, an analysis is first conducted on the correlations between the detrended preceding winter SST anomalies (hereafter referred to as SST) and WPSHRL (Figure 2). Consistent with previous studies, the Niño3.4 region (red-boxed area in Figure 2) provides the strongest indicative signal [28–32], and the linear

Preprints.org (www.preprints.org) | NOT PEER-REVIEWED | Posted: 16 January 2025 doi:10.20944/preprints202501.1259.v1

correlation coefficients between SST and WPSHRL can reach −0.48. This is the reason why the single-predictor method chooses the Niño3.4 index as predictor. Furthermore, it is noteworthy that the SST indicative signals are predominantly located in the Pacific and Indian oceans (blue-boxed area in Figure 2). Consequently, one multiple-predictor method extracts SST predictors from these regions instead of from the entire global oceans.

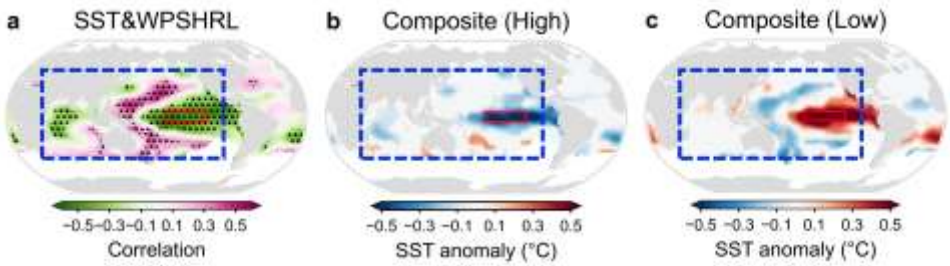

Figure 2. Correlation and composite analyses. (**a**) Spatial distribution of the linear correlation coefficients between SST and WPSHRL (stippling indicates the t-test confidence level greater than 95%). (**b**) Composite analysis of the SST in the high-WPSHRL years. (**c**) Composite analysis of the SST in the low-WPSHRL years. The red-boxed area is the Niño3.4 region, the blue-boxed area is the field of the Pacific and Indian oceans with strong indicative signals.

2.2. SST Predictor Extracting Methods

In this initial stage of the research on extracting multiple SST predictors, we explore two simple and feasible approaches: the ZONE approach and the EOF approach. Similar to the representative station [33–35], the ZONE approach selects 20 representative regions from the global SST field. The specific procedure is as follows: First, the SST grid with the largest year-to-year fluctuation is selected as the representative grid. Next, this representative grid and surrounding highly correlated grids are clustered together to form a single zone. Subsequently, this demarcated zone is taken out from the global SST field. This process is repeated until a total of 20 representative zones are established. The average SST of each zone serves as candidate predictors. Principal component analysis, also known as empirical orthogonal function (EOF) analysis, is a commonly used tool in climate studies [36–38]. Here, the EOF analysis is used to select SST predictors (i.e., EOF approach). The time series of 20 leading EOF spatial modes (i.e., EOF principal components) serve as candidate predictors. The predictors derived from the EOF approach are sourced from two different SST spatial areas: the entire global oceans (EOFg) and the preliminarily selected regions (blue-boxed area in Figure 2, EOFp). For convenience in comparison and reference, the four SST predictor extracting methods used in this study are listed in Table 1.

Table 1. Four SST predictor extracting methods.

Name	Number of predictors	Extracting approach	SST spatial area
Niño3.4	single	Niño3.4 index	Niño3.4 region
ZONE	multiple	representative zone	global oceans
EOFg	multiple	EOF	global oceans
EOFp	multiple	EOF	Pacific and Indian oceans

Figure 3 illustrates the 20 zones selected by the ZONE method, along with the corresponding SST time series. To clearly display the SST time series, only 6 representative zones that have the best correlation with WPSHRL are demonstrated. Because the ZONE approach prioritizes selecting the zone with the strongest SST fluctuation first, the ZONE number reflects the intensity of SST fluctuation. Consequently, the time series of ZONE1 and ZONE2 show relatively stronger amplitudes than the other zones. ZONE1 and ZONE2 are local in the central-eastern equatorial

Preprints.org (www.preprints.org) | NOT PEER-REVIEWED | Posted: 16 January 2025 doi:10.20944/preprints202501.1259.v1

Pacific and typically exhibit consistent signs of fluctuation. Besides ZONE1 and ZONE2 have strong correlations with WPSHRL (−0.48 and −0.54), ZONE7, ZONE9, ZONE11, and ZONE18 also show relatively strong correlations (absolute value more than 0.25). Because ZONE7, ZONE9, ZONE11, and ZONE18 are located far apart, their time series differ obviously from each other.

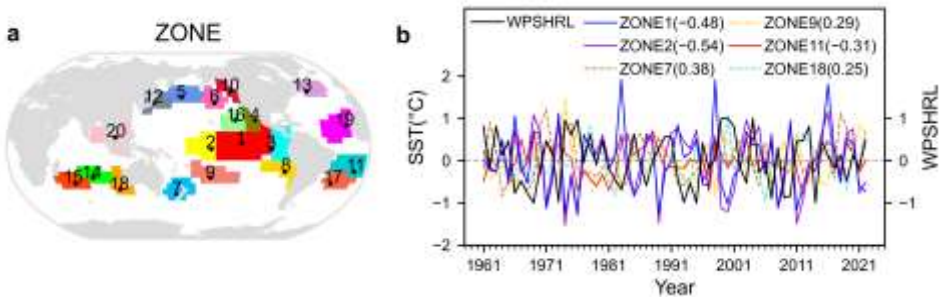

Figure 3. SST predictors extracted with the ZONE method. (**a**) Spatial distribution of the 20 zones (shading), with black dots representing the representative stations for each zone; (**b**) Time series of six zone SSTs (colored lines) and the WPSHRL (black line). The values in parentheses denote the correlation coefficients between these zone SSTs and WPSHRL.

Figure 4 illustrates the SST predictors extracted by the EOF approach. Regarding the global SST field (i.e., EOFg), the leading 20 EOF modes can explain 87.55% of the original SST field. Focusing on the area of the Pacific and Indian oceans (i.e., EOFp), the leading 20 EOF modes can explain 93.02% of the original field. Here, only the 6 EOF modes that have the best correlation with WPSHRL are shown. The first and third EOF modes from the EOFp method (i.e., EOFp1 and EOFp3) are generally consistent with those from the EOFg method (i.e., EOFg1 and EOFg3). Compared to EOFg1 (31.47%) and EOFg3 (6.18%), EOFp1 (41.71%) and EOFp3 (6.98%) contribute more to the original SST field. The linear correlation between EOFp3 and WPSHRL (−0.24) is slightly stronger than that of EOFg3 (−0.17). Taken overall, the time series of EOFp modes exhibit slightly stronger correlations with WPSHRL than that of EOFg modes. This can be explained by the fact that the preliminarily selected SST regions (i.e., Pacific and Indian oceans) used in the EOFp method exclude those SST regions lacking obvious indicative signals. Finally, it is important to note that the EOF modes and their corresponding time series are mutually orthogonal. This differs from the ZONE approach.

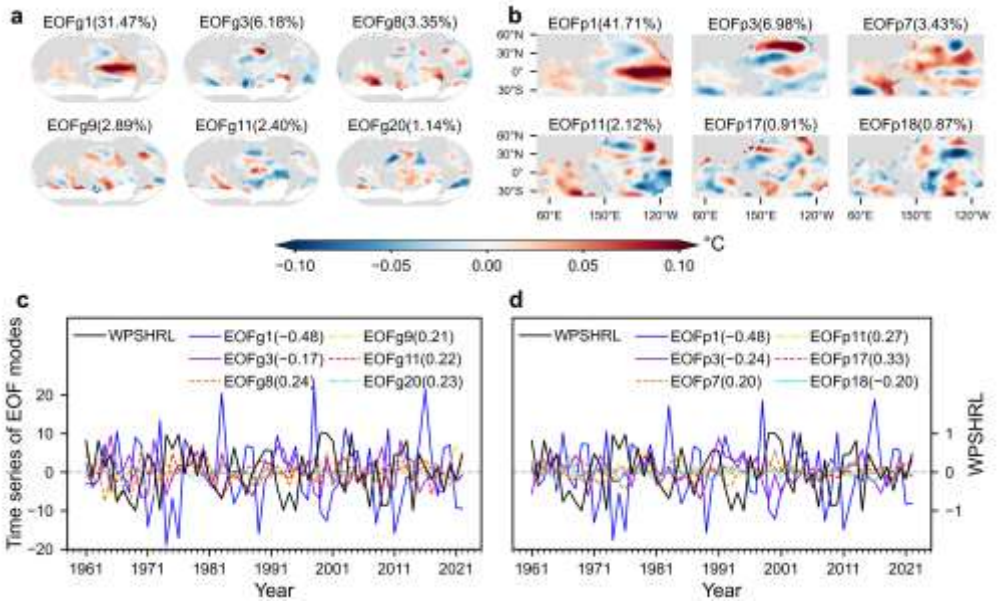

Preprints.org (www.preprints.org) | NOT PEER-REVIEWED | Posted: 16 January 2025 doi:10.20944/preprints202501.1259.v1

Figure 4. SST predictors extracted using the EOFg (**a**, **c**) and EOFp (**b**, **d**) methods. (**a**, **b**) Six EOF modes with the best correlation with WPSHRL. The fraction of variance explained by each mode is shown in parentheses. (**c**, **d**) Time series of the corresponding spatial modes (colored lines) and the WPSHRL (black line). The values in parentheses denote the correlation coefficients between these EOF modes and WPSHRL.

3. Forecast System and Estimating Method

The influence of SST predictor extracting methods on forecast skill may depend on the specific forecast model employed. To test this, two different regression models are employed in our forecast system: linear regression (LR) and neural network (NN). Given the potential for overfitting due to small sample sizes, forecast skill is estimated using rolling forecast experiments. Additionally, the forecast skill for anomaly events is also analyzed, as climate forecasts focus more on such events.

3.1. Forecast System

The climate forecast system developed by this study is a framework (i.e., the model parameters to be determined) that incorporates either LR or NN. Prior to conducting forecasts, these undetermined parameters (excluding hyperparameters) are established based on all available samples (i.e., samples before the predicted year). In other words, the relationship between SST and WPSHRL in the forecast system is continuously updated due to newly added samples from the latest year.

When using multiple-predictor methods, it is necessary to consider selecting a set of optimal predictors from the 20 SST variables. In the LR framework, this problem is solved by the stepwise regression method. Only predictors with a significant improvement on the predictand (i.e., WPSHRL) are retained while minimizing the number of predictors as much as possible to reduce the possibility of overfitting [39,40]. The technical details of stepwise regression can be found in the statistical textbooks [41,42].

The fundamental theory of the NN model can be found in the textbook about machine learning [43]. Here, we focus on illustrating how to use the NN model. Considering the limitation of sample size, the number of NN model parameters (i.e., the weights and biases associated with each layer) cannot be too large. Therefore, a shallow NN model with one hidden layer is chosen. There are two architecture hyperparameters for this NN framework: the number of input variables (Nin) and the number of neurons in the hidden layer (Nhid). The first Nin (Nin ≤ 20) SST variables that have the best correlation with WPSHRL are chosen as input predictors. Unlike the LR framework, which can calculate how many SST predictors (similar to Nin) are optimal for establishing a forecast model, the architecture hyperparameters for the NN framework (i.e., Nin and Nhid) need to be preset based on previous experience. We tested several architectures of the NN framework (hereafter Nin-Nhid), such as 4-2, 4-3, 6-2, 6-4, 8-4, 8-6, 10-4, 10-6, 12-4, and 12-6. The experiment results indicate that once Nin exceeds 6, there is no substantial enhancement in the forecast skill. Meanwhile, the influence of Nhid on the forecast skill is negligible. Therefore, the NN architecture is set to 6-4 for all the experiments shown in this study. It is noteworthy that, under the condition of small sample sizes, the performance of the NN model is unstable and sensitive to the random seeds for initialization [44]. Thus, using some techniques [24,45], this NN framework first selects 10 good seeds from 200 random seeds. Then, 10 NN models can be trained with these 10 good seeds, and the final output predictand is the average of the 10 corresponding predictands (i.e., ensemble mean). The stability of forecast results with the NN framework is shown in Figure A1.

3.2. Estimating Method

The rolling forecast technique is often used to estimate the forecast system [46–48]. Considering the limitation of sample years (1961 to 2022), the rolling forecast experiment used in this study consists of two parts: forward rolling forecast experiment (from 1992 to 2022) and backward rolling forecast experiment (from 1991 to 1961). In the forward rolling forecast experiment (i.e., the

Preprints.org (www.preprints.org) | NOT PEER-REVIEWED | Posted: 16 January 2025 doi:10.20944/preprints202501.1259.v1

commonly used rolling forecast), all available samples (from 1961 to the year before the predicted year) are used for the establishing forecast model. As for the backward rolling forecast experiment, the order of sample years is assumed to be reversed (from 2022 to the predicted year). To sum up, all sample years can be predicted by the rolling forecast experiment.

Forecast skill is usually quantified by the linear correlation coefficient (Cor) between observations and forecasts [49–52]. In this study, the probability of detection (POD) and false alarm rate (FAR) for anomaly events are also analyzed. The POD is defined as the ratio of the number of successfully predicted anomaly years to the total number of observed anomaly years and the FAR is defined as the ratio of the number of contradictory predicted anomaly years to the total number of anomaly years predicted by the forecast system [53–55]. Taken overall, the forecast skill is estimated by three scores (i.e., Cor, POD, and FAR).

4. Results and Analysis

Here, each SST multiple-predictor extracting method has a pair of rolling forecast experiments via both the LR and NN frameworks. Only the LR framework applies to the single-predictor method (i.e., univariate linear regression). For the convenience of expression, the names of SST extracting methods (i.e., Niño3.4, ZONE, EOFg, and EOFp) and the names of frameworks (i.e., LR and NN) are often used to label the corresponding experiments. We first show the comparison of these four SST extracting methods (Section 4.1), then explain these results through the sensitivity of the output predictand to input predictors described by forecast models (Section 4.2).

4.1. Forecast Skills

Figure 5 shows the influence of SST extracting methods on forecast skills. The LR experiments (i.e., based on the LR framework) show that one SST predictor (i.e., Niño3.4 index) could give a not-bad forecast once this predictor has a strong correlation with WPSHRL. The Niño3.4 experiment gives a better forecast skill (Cor 0.46, POD 4/31, FAR 0/8) than that from the EOFg experiment (Cor 0.31, POD 3/31, FAR 1/11). The main reason is that those SST areas without any indicative signals are put into every EOFg predictor (the entire global oceans). Unlike the EOFg predictors, the EOFp predictors do not have this disadvantage because they focus on the predominant signal regions (Pacific and Indian oceans). Therefore, the EOFp experiment improves the LR forecast skill (Cor 0.51, POD 11/31, FAR 1/17). The forecast skill from the LR experiment with ZONE predictors (Cor 0.49, POD 9/31, FAR 0/19) is also much better than that with EOFg predictors. One main reason is that only a few ZONE predictors significantly related to WPSHRL are incorporated into the LR forecast models even though these 20 zones are distributed globally. In summary, multiple SST predictors include not only more indicative signals but also more useless signals. As compared to a single strong predictor, the LR forecast skill based on multiple predictors might be improved due to more indicative signals. On the contrary, the forecast skill might worsen if too many useless signals are incorporated into the predictors.

Preprints.org (www.preprints.org) | NOT PEER-REVIEWED | Posted: 16 January 2025 doi:10.20944/preprints202501.1259.v1

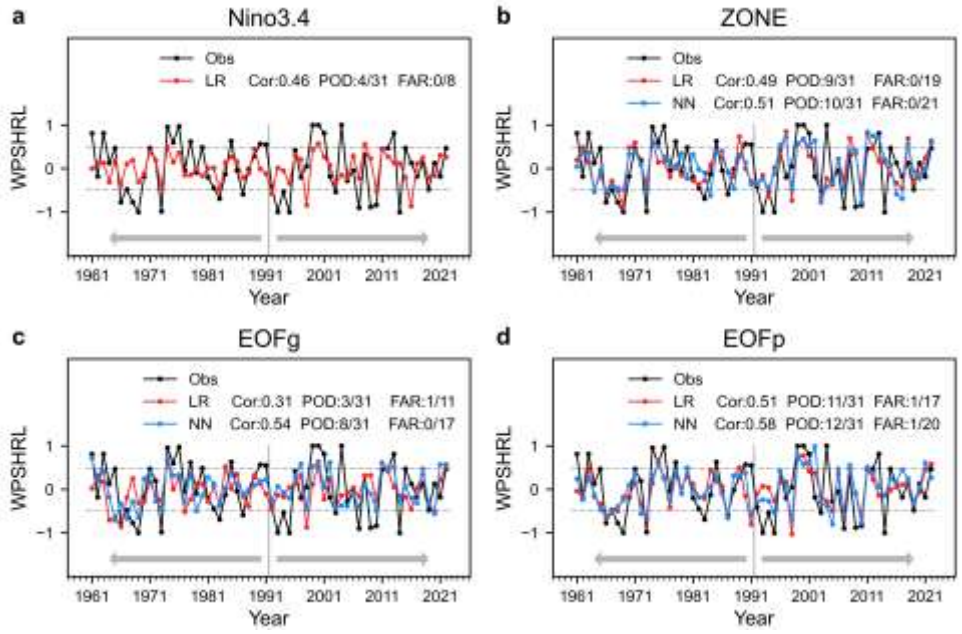

Figure 5. Rolling forecasts from the experiments with (**a**) the Niño3.4, (**b**) the ZONE, (**c**) the EOFg, and (**d**) the EOFp SST extracting methods. The observed WPSHRL is denoted by the black line. The red and blue lines indicate the forecasts from LR and NN models, respectively. Gray dashed lines indicate the threshold values for anomaly events. Forecast skills (Cor, POD, FAR) are presented next to the names of the forecast models.

This paragraph introduces the comparison between the NN framework and the LR framework (Figure 5). Both are based on the EOFg predictors, the forecast skill from NN models (Cor 0.54, POD 8/31, FAR 0/17) is much better than that from LR models (Cor 0.31, POD 3/31, FAR 1/11). It seems that the NN model can reduce the impact of useless signals mixed in the EOFg SST predictors. The ZONE and EOFp experiments also show that the forecast skills from NN models (Cor 0.51, POD 10/31, FAR 0/21; Cor 0.58, POD 12/31, FAR 1/20) are higher than those from LR models (Cor 0.49, POD 9/31, FAR 0/19; Cor 0.51, POD 11/31, FAR 1/17), especially for anomaly events. These analyses confirm that the NN model exhibits a better capacity to exploit the information provided by input predictors. Regarding the NN framework, there is a certain difference between the forecast skills of the ZONE and EOFp experiments. This might be caused by the fact that the EOFp SST predictors (the Pacific and Indian oceans) contain more information than the ZONE predictors (six zones in Figure 3a), and the orthogonal EOFp SST predictors are relatively easier to use. Taken overall, as compared to the LR models, the NN models could provide higher forecast skills and the differences in the NN forecast skills caused by multiple-predictor extracting methods (i.e., ZONE, EOFg, and EOFp) become small.

4.2. Sensitivity Analysis

The forecast skills only estimate the forecast system from the perspective of the final output predictands. Moreover, the relationship between the input predictors and the output predictand, which is characterized by the regression equation (i.e., the forecast model), constitutes an equally significant consideration. Here, the input-output relationships are investigated by the sensitivities of WPSHRL to the SST field, which can be calculated based on the established forecast model (i.e., model parameters have been determined). During the rolling forecast experiment, the forecast model undergoes an annual update (i.e., the model parameters differ each year) since the available samples used for model establishment are perpetually updated. Consequently, the sensitivity calculated based on the forecast model likewise demonstrates year-to-year variation.

The sensitivities derived from the LR forecast models of three years are presented in Figure 6. Typically, a handful of predictors are selected via the stepwise regression approach, and the predictors employed in the forecast model usually vary from year to year (Figure A2). This

Preprints.org (www.preprints.org) | NOT PEER-REVIEWED | Posted: 16 January 2025 doi:10.20944/preprints202501.1259.v1

phenomenon is manifested in the ZONE experiments. Take the year 2010 as an example, two zones are used in the forecast model. The sensitivities of these two zones are negative, and the two ZONE predictors (i.e., observed SST) also exhibit negative values. The inner product of input predictors and corresponding sensitivities determines the value of the output predictand. The sensitivities from the ZONE experiments indicate that the indicative information predominantly stems from the central-eastern equatorial Pacific region. This is in agreement with the highly correlated regions illustrated in Figure 2. Similarly, in the EOFg and EOFp experiments, the predicted value of WPSHRL is equivalent to the inner product of the observed SST field and the corresponding sensitivity field. Owing to the disparity in the spatial area between the EOFg and EOFp modes, the sensitivity fields from EOFg experiments are comparatively weak and fail to highlight the role of the central-eastern equatorial Pacific region. Consequently, in years with significant abnormalities (e.g., the years 1967 and 1999), the predicted WPSHRLs from the EOFg experiments are substantially weaker than those from the EOFp experiments. This constitutes the primary cause for why the LR experiment with EOFg predictors gives the poorest forecast skill in Figure 5. Overall, the SST-WPSHRL relationships represented by the sensitivity fields in Figure 6 exhibit certain differences among themselves; nonetheless, none of these relationships violate the linear statistical characteristic shown in Figure 2 (i.e., the common pattern from most years).

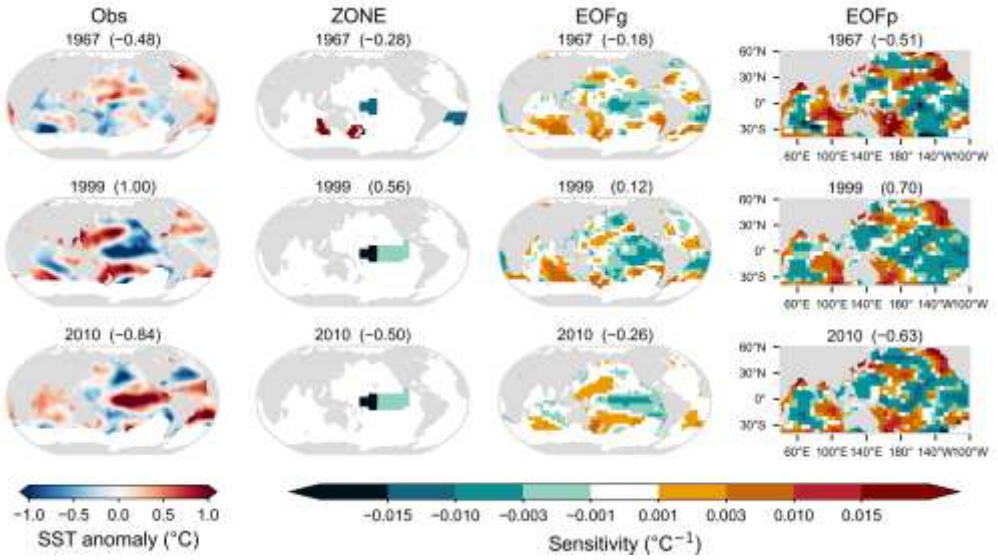

Figure 6. The preceding SST in three years (**left panel**) and corresponding sensitivities from the LR forecast models using three different SST extracting methods (**right panel**). The year numbers are shown at the top of each graph. The values in parentheses are the observed WPSHRL (**left panel**) and predicted WPSHRL (**right panel**).

Unlike the sensitivity from LR models which only depends on LR models themselves, the sensitivity from NN models also depends on the input predictors' state (i.e., the SST field used for the predicted year). For instance, in one established NN model, the Niño3.4 region sensitivity is influenced by the values of input SST over both the Niño3.4 region and other regions. This is consistent with the fact that the NN model can exploit more SST information for prediction (e.g., the coordination of each predictor). Figure 7 presents a comparison between LR models and NN models. In reference to the 1995 EOFp experiments, the sensitivity pattern from the NN model is somewhat similar to that from the LR model. Nevertheless, the NN model sensitivity is stronger than the LR model sensitivity, particularly over the central-eastern equatorial Pacific (the preceding SST indicative signal is very strong over there). Consequently, the NN model predicts a strong WPSHRL in comparison with the LR model. For the same reason, the 2013 EOFg experiments show a more obvious comparison between the LR model and the NN model. Regarding the 2001 ZONE experiments, both LR and NN models show positive sensitivity over the eastern Indian Ocean near

Preprints.org (www.preprints.org) | NOT PEER-REVIEWED | Posted: 16 January 2025 doi:10.20944/preprints202501.1259.v1

Australia. The preceding negative SST in this region induces a negative WPSHRL. In comparison with the LR model, the less positive NN model sensitivity is one reason for the higher WPSHRL predicted by the NN model. This also suggests that the NN model could flexibly incorporate the preceding SST information, subsequently improving the predicted WPSHRL.

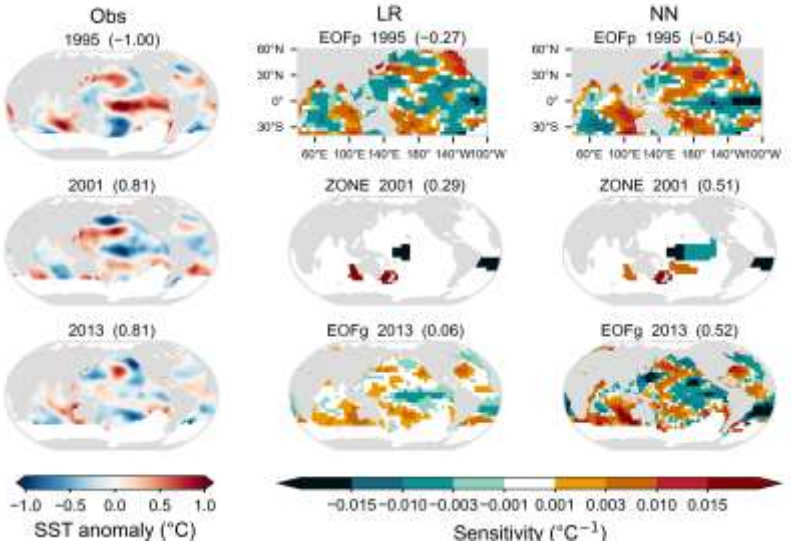

Figure 7. Similar to Figure 6, but for the comparison between LR models and NN models. The names of the forecast framework and SST extracting method are shown at the top of each graph.

5. Discussion

In the statistical climate forecast system developed by this study, the input predictors only come from SST. Besides SST, other meteorological elements might also be used in the forecast system, such as atmospheric circulation indexes [56,57]. This appears to contradict the previous theoretical studies, which confirm that the indicative signals for climate forecast mostly come from preceding SST [58]. In fact, there is no contradiction. The atmospheric circulation index used for climate forecast, in some ways, indicates the state of recent SST. In other words, this circulation index can be taken as a special SST predictor. This special SST information extracting method hinges on specific forecasted events. The specific events demand detailed discussion as they are not of a universal nature. Therefore, this special SST information extracting method is not investigated in this study.

6. Conclusions

The goal of this study is to gain experience in extracting SST predictors for the statistical climate forecast system. Based on the same climate forecast system, the comparison between different SST predictor extracting methods is investigated. To improve the robustness of research conclusions, two kinds of commonly used forecast models are employed in the climate forecast system: linear regression (LR) model and neural network (NN) model. This study investigates four predictor extracting methods: one single-predictor method (Niño3.4 index) and three multiple-predictor methods. The multiple predictors extracted from the EOF approach are orthogonal. In contrast to the multiple predictors extracted from the Pacific and Indian oceans, the multiple predictors extracted from the entire global oceans contain much more useless information for climate forecasting. Unlike the EOF approach, the multiple predictors extracted from the ZONE approach are non-orthogonal but have clear physical meaning.

As compared to a single strong SST predictor, multiple SST predictors contain not only more useful indicative information but also more useless information. Consequently, while multiple SST predictors can offer more information in comparison to a single predictor, the LR forecast model struggles to fully exploit this advantage. Meanwhile, the forecast skill from the LR model is sensitive

Preprints.org (www.preprints.org) | NOT PEER-REVIEWED | Posted: 16 January 2025 doi:10.20944/preprints202501.1259.v1

to the choice of multiple-predictor extracting methods. A primary determinant is whether these multiple predictors contain high quality information, so that the useful information far outweighs the useless information. Unlike the LR model, the NN model shows lower sensitivity to extracting methods because the NN model has a greater capacity in exploiting the useful information provided by input predictors. Moreover, the NN model could provide better forecast skills, especially for anomaly events. The comparison among these three sets of multiple predictors also suggests that whether multiple SST predictors are orthogonal might affect forecast skills. Among these three sets of multiple predictors investigated in this study, the orthogonal multiple predictors extracted from high-quality information regions show the best performance. In conclusion, this study offers valuable insights for the establishment of statistical climate forecast systems based on preceding SST data.

Author Contributions: X.S. designed this study. Y.C. built the forecast models, carried out the experiments, and created all figures. X.S. and Y.C. wrote the manuscript. All authors have read and agreed to the published version of the manuscript.

Funding: This research was funded by and the National Natural Science Foundation of China (grant nos. 41775095 and 42075145). The APC was funded by the same funders.

Institutional Review Board Statement: Not applicable.

Informed Consent Statement: Not applicable.

Data Availability Statement: The WPSHRL data were downloaded from http://cmdp.ncc-cma.net/160/74.php (accessed on 10 January 2025). The SST data were downloaded from https://psl.noaa.gov/data/gridded/data.kaplan_sst.html (accessed on 10 January 2025). The ERA5 reanalysis data were downloaded from https://climate.copernicus.eu/climate-reanalysis (accessed on 10 January 2025). The code of the forecast system and related results used in this study have been archived in a public repository https://doi.org/10.5281/zenodo.14638483 (accessed on 13 January 2025).

Acknowledgments: This study was conducted in the High-Performance Computing Center of Nanjing University of Information Science & Technology.

Conflicts of Interest: The authors declare no conflict of interest.

Appendix A

The rolling forecast experiments using the NN framework are executed three times, using the same code but different initialization random seeds, named 1st, 2nd, and 3rd. Both ZONE, EOFg, and EOFp experiments show that the differences among these three forecast results (i.e., 1st, 2nd, and 3rd) are relatively small (Figure A1). Generally speaking, the forecast system is relatively stable and experiment results are acceptable.

Preprints.org (www.preprints.org) | NOT PEER-REVIEWED | Posted: 16 January 2025 doi:10.20944/preprints202501.1259.v1

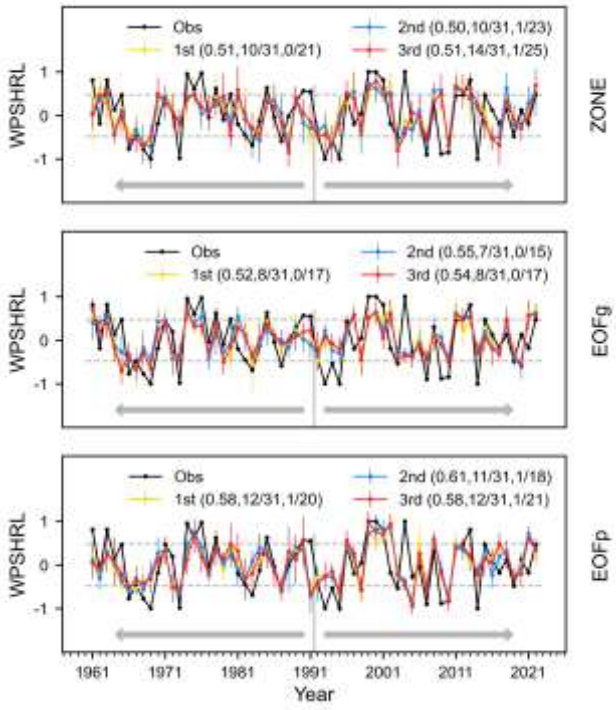

Figure A1. The stability of experiment results with the NN framework. The observed WPSHRL is denoted by the black line. The three colored lines indicate the forecasts using different initialization random seeds, respectively. Gray dashed lines indicate the threshold values for anomaly events. Forecast skills (Cor, POD, FAR) are presented next to the names of the experiments.

Appendix B

The number of SST predictors used in the rolling forecast experiments with the LR framework is illustrated in Figure A2. In the ZONE experiment, 4 predictors are most frequently utilized, and occurrences of more than 4 predictors are rare. One main reason is that ZONE predictors are not orthogonal. The fifth and subsequent predictors can be expressed by the previous predictors. In the EOFg experiment, 2 predictors are most commonly used. This can be explained by the fact that most EOFg predictors contain more useless information than useful information. Unlike the EOFg experiment, the EOFp experiment often uses more predictors.

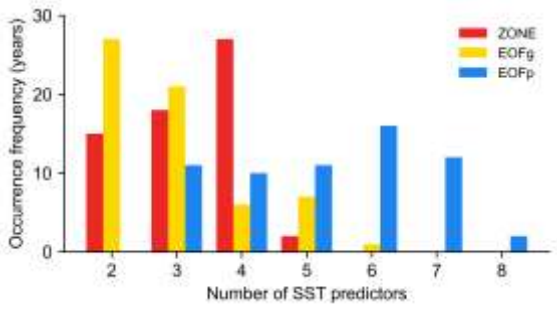

Figure A2. Occurrence frequency (in units of years) of different SST predictor numbers used in the rolling forecast experiments with the LR framework.

References

1. Zhou, T.; Yu, R. Atmospheric water vapor transport associated with typical anomalous summer rainfall patterns in China. *Journal of Geophysical Research: Atmospheres* **2005**, 110, D8. [CrossRef]

Preprints.org (www.preprints.org) | NOT PEER-REVIEWED | Posted: 16 January 2025 doi:10.20944/preprints202501.1259.v1

2. Ault, T.R.; Cole, J.E.; Evans, M.N.; Barnett, H.; Abram, N.J.; Tudhope, A.W.; Linsley, B.K. Intensified decadal variability in tropical climate during the late 19th century. *Geophysical Research Letters* **2009**, 36–8. [CrossRef]
3. Ren, H.; Zhang, F.; Luo, J.; Wang, R.; Liu, M.; Zhang, W.; Zhou, T.; Zhou, G. A Review of Research on Tropical Air-Sea Interaction, ENSO dynamics, and ENSO prediction in China. *Journal of Meteorological Research* **2020**, 34, 43–62. [CrossRef]
4. McPhaden, M.J.; Zebiak, S.E.; Glantz, M.H. ENSO as an integrating concept in earth science. *Science* **2006**, 314, 1740–1745. [CrossRef]
5. Chen, L.; Yuan, Y.; Yang M.; Zuo J.; Li W. A review of physical mechanisms of the global SSTA impact on EASM. *Journal of Applied Meteorological Science* **2013**, 24, 521–532. (In Chinese) [CrossRef]
6. Wang, H.; Ren, H.; Chen, H.; Ma, J.; Tian, B.; Sun, B.; Huang, Y.; Duan, M.; Wang, J.; Wang, L.; Zhou, F. Highlights of climate prediction study and operation in China over the past decades. *Acta Meteorologica Sinica* **2020**, 78, 317–331. (In Chinese) [CrossRef]
7. Ding, Y. Progress and prospects of seasonal climate prediction. *Advances in meteorological science and technology* **2011**, 1, 14–27. (In Chinese) [CrossRef]
8. Wei, F. Physical basis of short-term climate prediction in China and short-term climate objective prediction methods. *Journal of Applied Meteorological Science* **2011**, 22, 1–11. (In Chinese) [CrossRef]
9. Kosaka, Y.; Chowdary, J. S.; Xie S.; Min Y.; Lee, J. Limitations of seasonal predictability for summer climate over East Asia and the Northwestern Pacific. *Journal of Climate* **2012**, 25, 7574–7589. [CrossRef]
10. Zhou, B.; Wang, H. Relationship between the boreal spring Hadley circulation and the summer precipitation in the Yangtze River valley. *Journal of Geophysical Research* **2006**, 111, 1–14. [CrossRef]
11. Yun, K.; Seo, K.; Ha, K. Relationship between ENSO and northward propagating intraseasonal oscillation in the east Asian summer monsoon system. *Journal of Geophysical Research: Atmospheres* **2008**, 113, D14. [CrossRef]
12. Jiang, W.; Huang, G.; Huang, P.; Wu, R.; Hu, K.; Chen, W. Northwest Pacific anticyclonic anomalies during post-El Niño summers determined by the pace of El Niño decay. *Journal of Climate* **2019**, 32, 3487–3503. [CrossRef]
13. Huang, R.; Wu, Y. The influence of ENSO on the summer climate change in China and its mechanism. *Advances in Atmospheric Sciences* **1989**, 21–32. [CrossRef]
14. Wang, B.; Wu, R.; Fu, X. Pacific-East Asian teleconnection: How does ENSO affect east Asian climate? *American Meteorological Society* **2000**. [CrossRef]
15. Lin, Z.; Lu, R. The ENSO's effect on eastern China rainfall in the following early summer. *Advances in Atmospheric Sciences* **2009**, 26, 333–342. [CrossRef]
16. Wei, F. Progresses on climatological statistical diagnosis and prediction methods-in commemoration of the 50 anniversaries of CAMS establishment. *Journal of Applied Meteorological Science* **2006**, 736–742. (In Chinese) [CrossRef]
17. Cao, J.; Lu, R.; Hu, J.; Wang, H. Spring Indian Ocean-Western Pacific SST contrast and the East Asian summer rainfall anomaly. *Advances in Atmospheric Sciences* **2013**, 30, 1560–1568. [CrossRef]
18. Zhao, H. Analysis and prediction of the spatiotemporal characteristics of the interaction between the subtropical high and sea surface temperature. *Meteorological Monthly* **1986**, 21–23. (In Chinese) [CrossRef]
19. Chen, C.; Georgakakos, A.P. Seasonal prediction of East African rainfall. *International Journal of Climatology* **2015**, 35, 2698–2723. [CrossRef]
20. Liu, Y.; Fan, K. A new statistical downscaling model for autumn precipitation in China. *International Journal of Climatology* **2013**, 33, 1321–1336. [CrossRef]
21. Zhang, W.; Jin, F.; Stuecker, M.F.; Andrew, T.; Wittenberg, A.T.; Ren, H.; Kug, J.; Cai, W.; Cane, M. Unraveling El Nino's impact on the East Asian monsoon and Yangtze River summer flooding. *Geophysical Research Letters* **2016**, 43, 11375–11382. [CrossRef]
22. Qian, D.; Guan, Z.; Xu, J. Prediction models for summertime Western Pacific Subtropical High based on the leading SSTA modes in the tropical Indo-Pacific sector. *Transactions of Atmospheric Sciences* **2021**, 44, 405–417. (In Chinese) [CrossRef]

Preprints.org (www.preprints.org) | NOT PEER-REVIEWED | Posted: 16 January 2025 doi:10.20944/preprints202501.1259.v1

23. Huang, C.; Li, Q.; Xie, Y.; Peng, J. Prediction of summer precipitation in Hunan based on machine learning. *Transactions of Atmospheric Sciences* **2022**, 45, 191–202. (In Chinese) [CrossRef]
24. Sun, C.; Shi, X.; Yan, H.; Jiang, Q.; Zeng, Y. Forecasting the June Ridge Line of the Western Pacific Subtropical High with a Machine Learning Method. *Atmosphere* **2022**, 13, 660–660. [CrossRef]
25. Jiang, Q.; Shi X. Forecasting the July Precipitation over the middle-lower reaches of the Yangtze River with a flexible statistical model. *Atmosphere* **2023**,14, 152–152. [CrossRef]
26. Kaplan, A.; Cane, M.A.; Kushnir, Y.; Clement, A.C.; Blumenthal, M.B.; Rajagopalan, B. Analyses of global sea surface temperature 1856–1991. *Journal of Geophysical Research* **1998**, 103, 18567–18589. [CrossRef]
27. Liu, Y.; Li, W.; Ai, W.; Li, Q. Reconstruction and application of the monthly western Pacific subtropical high indices. *Journal of Applied Meteorological Science* **2012**, 23, 414–423. (In Chinese) [CrossRef]
28. Chen, L. Interaction between the subtropical high over the north pacific and the sea surface temperature of the eastern equatorial pacific. *Scientia Atmospherica Sinica* **1982**, 6, 148–156. (In Chinese) [CrossRef]
29. Zhao, Z.; Chen, G. The cause and forecast of long-term change of the latitudinal position of west pacific subtropical high in early summer. *Journal of Tropical Meteorology* **1995**, 223–230. (In Chinese) [CrossRef]
30. Ying, M.; Sun, S. A study on the response of subtropical high over the Western Pacific on the SST anomaly. *Chinese Journal of Atmospheric Sciences* **2000**, 24, 193–206. (In Chinese) [CrossRef]
31. Yao, Y.; Yan, H. Relationship between proceeding pacific sea surface temperature and subtropical high indexes of main raining seasons. *Journal of Tropical Meteorology* **2008**, 24, 483–489. (In Chinese) [CrossRef]
32. Kim, JE.E.; Yoo, C.; Park, S.H. Interdecadal change in the relationship between the western North Pacific subtropical high and the ENSO. *Theoretical and Applied Climatology* **2023**, 151, 1435–1447. [CrossRef]
33. Zhang, R.; Jiang, G.; Yu Z.; Jiang, Q. Establishment of prediction model for the pacific subtropical high using neural network calculation method. *Quarterly Journal of Applied Meteorology* **2000**, 474–483. (In Chinese) [CrossRef]
34. Qian, D.; Guan, Z.; Tang, W. Joint impacts of SSTA in tropical Pacific and Indian Oceans on variations of the WPSH. *Journal of Meteorological Research* **2018**, 32, 548–559. [CrossRef]
35. Wu, X.; Guo, S.; Ba, H.; He, S.; Xiong, F. Long-range precipitation forecasting based on multipole sea surface temperature. *ShuiLi XueBao* **2018**, 49, 1276–1283. (In Chinese) [CrossRef]
36. Richman, M.B. Principal component analysis in meteorology and oceanography. *American Meteorological Society* **1990**, 71, 212–214. [CrossRef]
37. Storch, H.; Zwiers, F.W.; Livezey, R.E. Statistical analysis in climate research. *Nature* **2000**, 404, 544. [CrossRef]
38. Mo, R.; Straus, M.D. Statistical-dynamical seasonal prediction based on principal component regression of GCM ensemble integrations. *American Meteorological Society* **2002**, 130, 2167–2187. [CrossRef]
39. Zhang, J.; Zhao, Q.; Xu, X. Methods for Combining Predictors in Statistical Forecasting. *Scientia Atmospherica Sinica* **1978**, 48–54. (In Chinese) [CrossRef]
40. Wilks, D.S. *Statistical Methods in the Atmospheric Sciences*, 3rd ed.; Academic Press: London, UK, 2006; pp. 235–312. [CrossRef]
41. Derksen, S.; Keselman, H.J. Backward, forward and stepwise automated subset selection algorithms: Frequency of obtaining authentic and noise variables. *British Journal of Mathematical and Statistical Psychology* **1992**, 45, 265–282. [CrossRef]
42. Kutner, M.H.; Nachtsheim, C.J.; Neter, J.; Li, W. *Applied linear statistical models*. McGrawhill, 2005. [CrossRef]
43. Goodfellow, I.; Bengio, Y.; Courville, A. *Deep Learning*; MIT Press: Cambridge, CA, USA, 2016; pp. 89–223. [CrossRef]
44. Dodge, J.; Ilharco, G.; Schwartz, R.; Farhadi, A.; Hajishirzi, H.; Smith, N. Fine-tuning pretrained language models: Weight initializations, data orders, and early stopping. *arXiv* **2020**, arXiv:2002.06305. [CrossRef]
45. Snieder, E.; Abogadil, K.; Khan, U.T. Resampling and ensemble techniques for improving ANN-based high-flow forecast accuracy. *Hydrology and Earth System Sciences* **2021**, 25, 2543–2566. [CrossRef]
46. Mao, W.; Chen, Y.; Bai, S.; Li, W. Experiment of running prediction of precipitation in flood period in China with ensemble analysis of physical-statistic prediction. *Meteorological Monthly* **2011**, 37, 547–554. (In Chinese) [CrossRef]

Preprints.org (www.preprints.org) | NOT PEER-REVIEWED | Posted: 16 January 2025 doi:10.20944/preprints202501.1259.v1

47. Huang, X.; He, L.; Zhao, H.; Huang, Y.; Wu, Y. Application of shapley-fuzzy neural network method in long-time rolling forecasting of typhoon satellite image in South China. *Acta Meteorologica Sinica* **2021**, 79, 309–327. (In Chinese) [CrossRef]
48. Tian, W.; Song, P.; Chen, Y. Short-term rolling prediction of tropical cyclone intensity based on multi-task learning with fusion of deviation-angle variance and satellite imagery. *Advances in Atmospheric Sciences* **2024**, 42, 111–128. [CrossRef]
49. Zhu, C.; Park, C.K.; Lee, W.S.; Yun, W.T. Statistical downscaling for multi-model ensemble prediction of summer monsoon rainfall in the Asia-Pacific region using geopotential height field. *Advances in Atmospheric Sciences* **2008**, 25, 867–884. [CrossRef]
50. Ke, Z.; Zhang, P.; Dong, W.; Wang, J. An application of optimal subset regression in seasonal climate prediction. *Chinese Journal of Atmospheric Science* **2009**, 33, 994–1002. (In Chinese) [CrossRef]
51. Ren, H.L.; Jin, F.F.; Song, L.; Lu, B.; Tian, B.; Zuo, J.; Liu, Y.; Wu, J.; Zhao, C.; Nie, Y.; Zhang, P.; Ba, J.; Wu, Y.; Wan, J.; Yan, Y.; Zhou, F. Prediction of primary climate variability modes at the Beijing Climate Center. *Journal of Meteorological Research* **2017**, 31, 204–223. [CrossRef]
52. Liu, Y.; Ren, H.; Zhang, P.; Zuo, J.; Tian, B.; Wan, J.; Li, Y. Application of the hybrid statistical downscaling model in summer precipitation prediction in China. *Climatic and Environmental Research* **2020**, 25, 163–171. (In Chinese) [CrossRef]
53. Chen, F.; Li, X. Evaluation of IMERG and TRMM 3B43 monthly precipitation products over mainland China. *Remote Sensing* **2016**, 8, 472. [CrossRef]
54. Chen, C.; Chen, Q.; Duan, Z.; Zhang, J.; Mo, K.; Li, Z.; Tang, G. Multiscale comparative evaluation of the GPM IMERG v5 and TRMM 3B42 v7 precipitation products from 2015 to 2017 over a climate transition area of China. *Remote Sensing* **2018**, 10, 944. [CrossRef]
55. Frnda, J.; Durica, M.; Nedoma, J.; Zabka, S.; Martinek, R.; Kostelansky; M. A weather forecast model accuracy analysis and ECMWF enhancement proposal by neural network. *Sensors* **2019**, 19, 5144. [CrossRef]
56. Fan, K.; Lin, M.J.; Gao, Y.Z. Forecasting the summer rainfall in North China using the year-to-year increment approach. *Science in China Series D: Earth Science* **2009**, 52, 532–539. [CrossRef]
57. Wu, Y.; Tang, H.; Liu, Y.; Dong, X.; Guo, Q. Application of statistical downscaling model to Autumn rainfall forecasting over southwest China. *Meteorological Monthly* **2020**, 46, 1555–1564. [CrossRef]
58. Kalnay, E. *Atmospheric Modeling, Data Assimilation and Predictability*. Cambridge University Press, 2003, 341. [CrossRef]

Disclaimer/Publisher's Note: The statements, opinions and data contained in all publications are solely those of the individual author(s) and contributor(s) and not of MDPI and/or the editor(s). MDPI and/or the editor(s) disclaim responsibility for any injury to people or property resulting from any ideas, methods, instructions or products referred to in the content.